
How Sensitive Is the Upper Gastrointestinal Tract to ^{90}Y Radioembolization? A Histologic and Dosimetric Analysis in a Porcine Model

Alexander S. Pasciak^{1,2}, Laurentia Nodit³, Austin C. Bourgeois^{1,4}, Ben E. Paxton⁵, Patricia N. Coar⁶, Christopher T. Clark³, M. Katherine Tolbert⁷, Joleen K. Adams⁶, Aravind Arepally^{8,9}, and Yong C. Bradley¹

¹Department of Radiology, University of Tennessee Graduate School of Medicine, Knoxville, Tennessee; ²The Johns Hopkins Hospital, School of Medicine, Baltimore, Maryland; ³Department of Pathology, University of Tennessee Graduate School of Medicine, Knoxville, Tennessee; ⁴Department of Radiology, The Medical University of South Carolina, Charleston, South Carolina; ⁵Interventional Radiology, Prescott Radiologists, Prescott, Arizona; ⁶Office of Lab Animal Care, University of Tennessee College of Veterinary Medicine, Knoxville, Tennessee; ⁷Department of Small Animal Clinical Sciences, University of Tennessee College of Veterinary Medicine, Knoxville, Tennessee; ⁸Interventional Radiology, Piedmont Radiology, Atlanta, Georgia; and ⁹Interventional Radiology, Vanderbilt School of Medicine, Nashville, Tennessee

In ^{90}Y radioembolization, nontarget embolization to the stomach or small bowel can result in gastrointestinal injury, a rare but difficult to manage clinical complication. However, dosimetric thresholds for toxicity to these tissues from radioembolization have never been evaluated in a controlled setting. We performed an analysis of the effect of ^{90}Y radioembolization in a porcine model at different absorbed-dose endpoints. **Methods:** Six female pigs underwent transfemoral angiography and infusion of ^{90}Y -resin microspheres into arteries supplying part of the gastric wall. Esophagogastroduodenoscopy was performed after 4 wk to assess interim gastrointestinal health. Animals were monitored for side effects for 9 wk after ^{90}Y infusion, after which they were euthanized and their upper gastrointestinal tracts were excised for analysis. Histologic sections were used to map microsphere location, and a microdosimetric evaluation was performed to determine the absorbed-dose profile within the gastrointestinal wall. **Results:** ^{90}Y radioembolization dosages from 46.3 to 105.1 MBq were infused, resulting in average absorbed doses of between 35.5 and 91.9 Gy to the gastric wall. No animal exhibited any signs of pain or gastrointestinal distress through the duration of the study. Excised tissue showed 1–2 small (<3.0 cm²) healed or healing superficial gastric lesions in 5 of 6 animals. Histologic analysis demonstrated that lesion location was superficial to areas of abnormally high microsphere deposition. An analysis of microsphere deposition patterns within the gastrointestinal wall indicated a high preference for submucosal deposition. Dosimetric evaluation at the luminal mucosa performed on the basis of microscopic microsphere distribution confirmed that ^{90}Y dosimetry techniques conventionally used in hepatic dosimetry provide a first-order estimate of absorbed dose. **Conclusion:** The upper gastrointestinal tract may be less sensitive to ^{90}Y radioembolization than previously thought. Lack of charged-particle equilibrium at the luminal mucosa may contribute to decreased toxicity of ^{90}Y radioembolization compared with external-beam radiation therapy in gastrointestinal tissue. Clinical examples of injury from ^{90}Y nontarget embolization have likely resulted from relatively large ^{90}Y

activities being deposited in small tissue volumes, resulting in absorbed doses in excess of 100 Gy.

Key Words: ^{90}Y ; radioembolization; interventional oncology; SIRT

J Nucl Med 2016; 57:1957–1963

DOI: 10.2967/jnumed.116.176768

One of the most severe side effects from ^{90}Y radioembolization in the treatment of liver cancer is gastrointestinal complication, including ulceration. Postradioembolization-induced gastrointestinal ulceration may occur after nontarget embolization (NTE) of radioactive microspheres into arteries supplying the esophagus, stomach, or duodenum, including the gastroduodenal artery, right-gastric artery, or other gastroenteric collaterals. Although the availability of published data is limited, incidence rates of gastrointestinal ulceration after hepatic ^{90}Y radioembolization are on the order of 3% (1).

Despite the rarity of gastrointestinal ulceration, aggressive prophylaxis is directed toward preventing these complications, as coil occlusion of the gastroduodenal and right-gastric arteries are considered in pretreatment radioembolization planning. However, because coil occlusion often carries the consequence of formation of additional hepatoenteric collaterals (2), balloon occlusion techniques (3) or antireflux catheters (4) have also been used to prevent gastrointestinal complication. This substantial effort directed toward prophylaxis may be in part due to the severity and purported difficulty in managing these complications (5).

Little is known about the radiation biology and thresholds for gastrointestinal injury after radioembolization, likely secondary to the difficulty in determining tissue-absorbed doses in the limited cases in which these complications occurred. However, data from external-beam radiation therapy (EBRT) suggest that the stomach/small bowel may actually be less radiosensitive than the liver. The accepted 50% perforation or ulceration rate at 5 y (TD_{50/5}) after external-beam irradiation of the stomach/small bowel is 50–60 Gy (6), whereas the TD_{50/5} for liver failure is only 35 Gy for whole-liver irradiation (7). Of course, the hepatic TD_{50/5} is markedly

Received Apr. 15, 2016; revision accepted Jun. 7, 2016.
For correspondence or reprints contact: Alexander S. Pasciak, The Johns Hopkins School of Medicine, 733 N. Broadway, Baltimore, MD 21205.
E-mail: alexander.pasciak@gmail.com
Published online Jul. 7, 2016.
COPYRIGHT © 2016 by the Society of Nuclear Medicine and Molecular Imaging, Inc.

different for ^{90}Y radioembolization than EBRT, because the maximum recommended absorbed dose to normal liver is 70 and 120 Gy for resin and glass microspheres, respectively (8,9). This discrepancy is explained by many factors including dose rate, partial liver irradiation (10), and microscopic absorbed-dose inhomogeneity (11). Therefore, whereas data exist on the toxicity thresholds of EBRT on the stomach and small bowel (6), direct application of these data to radioembolization may not be possible.

In this study, we used a porcine model to assess the relationship between ^{90}Y radioembolization absorbed dose and toxicity in the upper gastrointestinal tract.

MATERIALS AND METHODS

The University of Tennessee College of Veterinary Medicine Institutional Animal Care and Use Committee approved the animal protocol used in this experiment. Six female pigs (age, 12–13 wk; weight, 21.8–28.1 kg) were included in this study. All diagnostic and angiographic procedures were performed under general anesthesia. Telazol and xylazine (4.4 mg/kg for telazol and 2.2 mg/kg for xylazine; Zoetis Inc. and Bayer, respectively) were used as a preanesthetic, and anesthesia was maintained with a 1%–5% isoflurane inhalant (Baxter Health Care Corp.) with 100% oxygen after endotracheal tube placement. All animals received a calibrated infusion of ^{90}Y -resin microspheres (SIR-Spheres, SIRTex Medical Ltd.), with 3 of these animals randomly selected to receive a diagnostic procedure before radioembolization. Before all surgical interventions, an intramuscular injection of penicillin (10,000 IU/kg; AGRI-Cillin [Agri-Labs]) was administered, and a fentanyl transdermal patch (50 ug/h; Duragesic [Alza Corp.]) was applied for preemptive analgesia.

$^{99\text{m}}\text{Tc}$ -Macroaggregated Albumin (MAA) Infusion and CT Imaging

On the basis of extrapolation of EBRT data (6), absorbed doses of up to 100 Gy were selected as a reasonable starting point for investigation into the gastrointestinal toxicity of radioembolization. However, because of the small duodenal wall tissue volume, infusion of less than 20 MBq of ^{90}Y would be required to reach an absorbed dose of 100 Gy. Controlled administration of dosages on this scale could not be performed accurately using a clinical ^{90}Y radioembolization delivery system designed to infuse GBq dosages. Therefore, the stomach fundus was selected as the tissue target for determining gastrointestinal sensitivity to radioembolization because a greater tissue volume was available and angiographic techniques for fundal particle embolization in a porcine model have been previously described (12).

After conventional ^{90}Y radioembolization treatment planning, a $^{99\text{m}}\text{Tc}$ -MAA infusion, nuclear scintigraphy, and CT volumetry were used to determine perfused tissue volumes for treatment planning in 3 animals (Table 1). Ultrasound guidance was used to obtain percuta-

neous femoral access. A 5-French Cobra (Surefire Medical) catheter was advanced into the celiac artery, followed by angiography to map the arteries supplying the gastric fundus. Following established techniques (12), a 2.8-French microcatheter (Precision Microcatheter; Surefire Medical) was advanced into the main left gastric and the gastric artery arising from the splenic artery, reflecting the 2 primary arteries supplying the lateral and medial boundaries of the stomach fundus. $^{99\text{m}}\text{Tc}$ -MAA (120 ± 10 MBq) was infused into each artery. All angiographic procedures were performed by board-certified interventional radiologists using a Veradius Neo (Philips Healthcare) vascular C-arm.

After infusion of $^{99\text{m}}\text{Tc}$ -MAA, 4-view scintigraphy was performed on an ADAC Argus γ -camera, followed by a contrast-enhanced abdominal CT scan on a Brilliance (Philips Healthcare) 40-slice system. A dual-board-certified diagnostic and nuclear medicine radiologist contoured perfused tissue volume on CT data reconstructed with a 0.5-mm slice thickness. Planar scintigraphic images were cross-referenced with reformatted CT scans to determine the coverage of MAA; however, limiting volumetry only to CT ensured high resolution and accurate tissue volume determination. A 3-dimensional interpolative spline-contouring algorithm was used to determine tissue volume (Osirix 64; Pixemo).

Perfused tissue volume per unit of animal weight was consistent in animals 1–3 (2.57 ± 0.12 cm³/kg, Table 1). Therefore, these estimates were applied to animals 4–6 using Equation 1 after angiographic verification of identical fundal vasculature among all animals.

$$V_{F,t} (\text{cm}^3) = \frac{M_t (\text{kg})}{3} \sum_{i=A,C,G} V_{F,i} (\text{cm}^3) / M_i (\text{kg}), \quad \text{Eq. 1}$$

where $V_{F,t}$ is the calculated perfused stomach volume of animals 4–6, $V_{F,i}$ is the measured perfused stomach volume of animals 1–3, and M is the weight of the animal at the time of treatment.

Dosage Determination

Treatment planning for ^{90}Y -microsphere infusion was performed assuming uniform deposition of ^{90}Y -microspheres in the measured tissue volume. Equation 2 was adapted from the MIRD formalism for hepatic radioembolization (13).

$$D_{\text{avg}} (\text{Gy}) = \frac{A_0 (\text{MBq}) \times 49.86 (\text{J} \cdot \text{s})}{M_{\text{tissue}} (\text{g})} = \frac{A_0 (\text{MBq}) \times 49.86 (\text{J} \cdot \text{s})}{V_f (\text{cm}^3) \times 1.03 \left(\frac{\text{g}}{\text{cm}^3}\right)}, \quad \text{Eq. 2}$$

where D_{avg} is the expected average absorbed dose to tissue, M_{tissue} is the mass of the treated stomach tissue, and A_0 is the infused ^{90}Y radioactivity. Average absorbed-dose endpoints (D_{avg}) for treated animals based on Equation 2 ranged from 35.5 to 91.9 Gy (Table 2). The authors acknowledge that the use of the MIRD hepatic dosimetry technique (Eq. 2) for gastrointestinal dosimetry is associated with several flaws, to be discussed.

TABLE 1
CT Volumetry Data

Animal no.	Gastrointestinal infusion	Preprocedural weight (kg)	Perfused stomach volume (cm ³)	Volume per unit animal weight (cm ³ /kg)
1	$^{99\text{m}}\text{Tc}$ -MAA/ ^{90}Y	25.8	68	2.63
2	$^{99\text{m}}\text{Tc}$ -MAA/ ^{90}Y	25.9	63	2.43
3	$^{99\text{m}}\text{Tc}$ -MAA/ ^{90}Y	28.1	74	2.63

TABLE 2
Treatment Dosages and D_{avg} for All Animals

Animal	Gastrointestinal infusion	Perfused stomach volume (cm ³)	A_0 (MBq)	D_{avg} (Gy) (MIRD, Equation 2)
1	^{99m} Tc-MAA/ ⁹⁰ Y	68	48.4	35.5
2	^{99m} Tc-MAA/ ⁹⁰ Y	63	46.3	36.6
3	^{99m} Tc-MAA/ ⁹⁰ Y	74	75.5	50.9
4	⁹⁰ Y	60	66.2	55.0
5	⁹⁰ Y	64	95.5*	*
6	⁹⁰ Y	57	105.1	91.9

*During infusion, pressurization across gastroepiploic artery caused nontarget deposition of unknown portion of infused dosage directed to nontarget tissue.

Infusion of ⁹⁰Y into Stomach

Identical angiographic procedures were followed for infusion of ⁹⁰Y-microspheres, which took place the day after the ^{99m}Tc-MAA infusion/volumetry. Although the stomach has substantially larger tissue volume than the duodenum, the infused activities were less than one tenth of traditional GBq treatment dosages used in hepatic radioembolization (Table 2). To facilitate accurate administration of these small activities, a prototype resin-microsphere infusion system (MixSIR; SIRTeX Medical Ltd.) was used. The MixSIR oscillates resin microspheres contained in a 60-cm³ syringe maintaining uniform suspension and provides a linear activity administration per unit volume infused. An activity concentration of approximately 5 MBq/cm³ in the syringe allowed for administration of the dosages in Table 2.

Care and Monitoring

All animals received twice-daily monitoring by a study veterinarian for clinical signs indicative of gastric distress including loss of appetite, signs of nausea, emesis, diarrhea, melena, hematochezia, and behavior change. Omeprazole (1 mg/kg) was administered orally twice weekly for the duration of the study to replicate standard-of-care prophylaxis given to any patient believed to have received gastrointestinal ⁹⁰Y NTE. Four weeks after infusion of ⁹⁰Y radioembolization, esophagogastroduodenoscopy was performed by an investigator masked to treatment in left lateral recumbency to evaluate gastrointestinal status and interim healing.

Poststudy Histopathologic Analysis

Animals 1–3 and 4–6 were euthanized 69 and 74 d, respectively, after ⁹⁰Y radioembolization with intravenous administration of Fatal-Plus solution at 0.25 mL/kg (Vortech Pharmaceuticals). The stomach was excised from each animal and opened along the greater curvature and fixed overnight in 10% formalin solution. Gross examination including documentation of any lesions with respect to size, location, and degree of activity was performed both before and after fixation. All areas of noted mucosal lesions, active or healed, in addition to representative tissue sections of the esophagus, gastroesophageal junction, and stomach (including fundus, body, and antrum) were submitted in their entirety for histologic examination.

Histologic sections were stained with hematoxylin and eosin (H&E) and Masson trichrome via standard technique. All H&E- and trichrome-stained sections were scanned on an Aperio FL slide scanner (Leica Biosystems Inc.). The thickness of the gastric wall and location of microsphere clusters relative to their distance from the lumen were measured using scanned sections and then used to construct a probability function of microsphere deposition. Around each

cluster, the extent of fibrosis was measured on trichrome sections. Because fibrosis extended from microsphere clusters both toward the lumen and toward the serosa in a banding pattern, the visible edges of fibrosis extending in each direction was measured, relative to each cluster, for comparison to the microdosimetric evaluation described below.

Dose Profile Assessment

The validity of the MIRD method for hepatic dosimetry (13) was assessed in the gastrointestinal wall with a dose-point kernel (DPK) computed using MCNP6 in 100- μ m voxels. Electron/photon-coupled Monte Carlo transport of 10⁸ histories was performed using the ⁹⁰Y β -spectrum as defined by Eckerman (14), with the source uniformly distributed within the central 100- μ m voxel (Fig. 1). Dose profiles were computed using convolution-based dosimetry with the DPK in a slab-geometry representation of the stomach wall using 2 methods. The first method assumed uniform microsphere deposition within the entire stomach wall, maintaining consistency with the uniformity assumed in the MIRD model for hepatic ⁹⁰Y dosimetry, but accounting for lack of charged-particle equilibrium (CPE). The second method accounted for nonuniform deposition of microspheres within the stomach wall by convolving the DPK with the measured probability function of microspheres depositing at different distances relative to the lumen, as determined from histologic measurement. In both methods, the stomach contents also were simulated as soft tissue, rather than gas, to allow for convolution-based dosimetry.

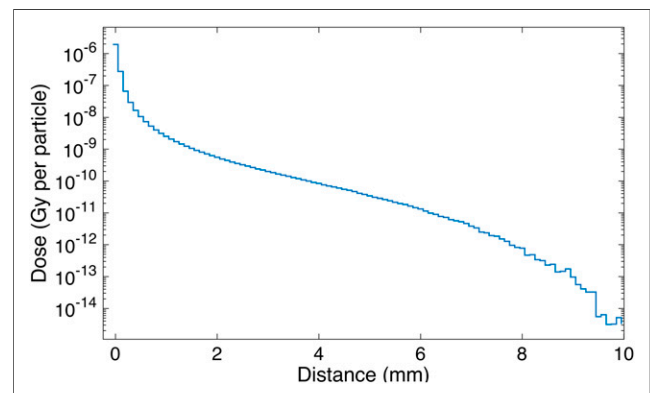


FIGURE 1. Voxel values for 100- μ m DPK along (0,0,1) unit vector. Source voxel is centered at (0,0,0) and contains uniform ⁹⁰Y distribution. Because of small voxel size, noise is present at distances approaching 1 cm despite large number of histories run.

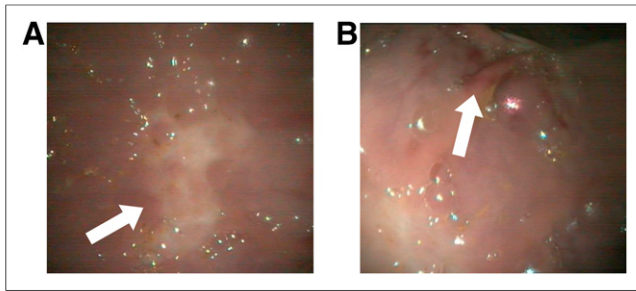


FIGURE 2. Endoscopy of pig 3 at 4 wk after radioembolization. (A) Fibrosis is clearly visible from potentially already healed lesion (arrow). (B) Several superficial mucosal erosions are apparent (arrow).

TABLE 3
Gross-Pathologic Findings in Each Pig

Animal no.	No. of lesions	Lesion size and active status
1	0	—
2	1	1.5 × 1 cm, healed
3	2	1 × 0.9 cm, healed 2 × 1.5 cm, healed
4	2	1.9 × 0.5 cm, active; crater size, 0.9 × 0.08 × 0.06 cm 2 × 0.5 cm, healed
5	1	2.5 × 0.2 cm, active; crater size, 0.3 × 0.14 × 0.12 cm
6	1	0.9 × 0.6 cm, healed

RESULTS

^{90}Y dosages from 46.3 to 105.1 MBq were infused into the gastric wall of 6 pigs, representing D_{avg} between 35.5 and 91.9 Gy, using the formalism in Equation 2 (Table 2). All $^{99\text{m}}\text{Tc-MAA}$ and ^{90}Y infusion procedures were performed without complication, except for the ^{90}Y infusion on pig 5. During this procedure, pressurization across the gastropoploic artery caused an unknown portion of the dosage to be directed to nontarget tissue. Therefore, the actual dosage of radioactivity delivered to the expected perfused gastrointestinal tissue volume in this animal was unknown (Table 2).

After infusion of ^{90}Y -microspheres, no animal showed any loss of appetite, signs of dyspepsia, emesis, melena, or hematochezia

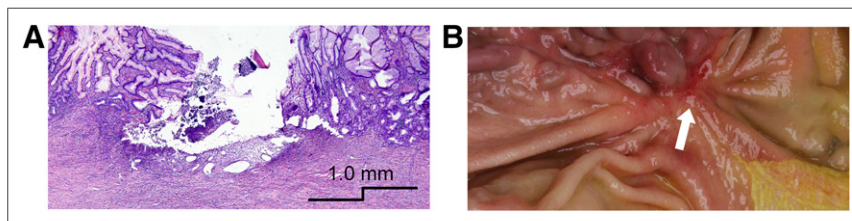


FIGURE 3. Gross and histologic analyses of 1.9 × 0.3 cm lesion in pig 4 after euthanasia. (A) H&E section showing superficial active crater. Increased collagen deposition and significant fibrosis is apparent, involving both mucosa and submucosal layer. (B) Gross image of lesion (arrow) before formalin fixation.

throughout the trial. Energy level and socialization habits of the animals as evaluated by study veterinarians did not change at any point during the study.

Endoscopy and Gross Pathology

Endoscopy showed prominent vascularity and pinpoint multifocal discolorations in the stomachs of all pigs undergoing esophagogastroduodenoscopy. The lesion severity correlated positively with dose of radiation. At D_{avg} greater than 50 Gy (Table 2), erosions were present in treated areas with mild mucosal hemorrhage. No areas were scored as ulcers according to criteria previously published (15). Areas of fibrosis, however, could be visually appreciated (Fig. 2).

After euthanasia, gross mucosal abnormalities could be easily appreciated. Abnormalities were present in pigs 2–6 (Table 3). Pigs 2, 3, and 6 had 1 or 2 healed superficial mucosal lesions, located in the treated gastric wall. The lesions observed in pigs 4 and 5 were predominantly healed but had a small central active crater showing mucosal necrosis and hemorrhage. No transmural perforations were appreciated. The largest remaining active lesion at the time of euthanasia (pig 4, Table 3) was sectioned and had an active region with a depth of 0.8 mm (Fig. 3). The mucosa exhibited a nodular and rough appearance, which was also noted endoscopically. This finding was more prominent in animals with a D_{avg} exceeding 50 Gy.

Histopathology

H&E sections demonstrated that all animals had a mild chronic gastritis characterized by large lymphoid aggregates and increased chronic inflammation in the lamina propria. Sections confirmed the presence of resin microspheres, which stained significantly darker than the gastric tissue and were easily visible. Deposition of microspheres in gastrointestinal tissue was inhomogeneous, with a cluster pattern similar to that of liver and tumor radioembolization, previously reported (16). Five of 6 animals demonstrated signs of minimally active, healing, or fully healed mucosal lesions, superficial to areas with higher submucosal microsphere density. In these regions, there was mucosal atrophy and increased collagen deposition involving both mucosa and submucosal layer (Fig. 4). Histologic signs usually associated with acute radiation injury, such as multinucleation, cytomegaly, atypia, apoptosis, or increased mitoses, were not appreciated.

Microspheres were found to deposit inhomogeneously in the tissue layers of the stomach. Spheres formed clusters ranging in size from 30 to 600 μm with between 2 and 100 microspheres per cluster. Predominant deposition of microspheres was observed from the base of the crypts in the mucosa to the muscularis mucosae, with the highest concentration in the submucosa. Few clusters were observed entrapped in the muscularis propria and subserosa. Microspheres deposited in a periarteriolar fashion, eliciting minimal foreign body giant cell reaction. Mean cluster-to-lumen distance measured from 467 independent microsphere clusters (2,963 microspheres) in all 6 treated pigs was 2.3 ± 1.6 mm, with 76% of identified clusters localized in the submucosa. Figure 5 shows a histogram describing the distance from the lumen of each measured microsphere cluster.

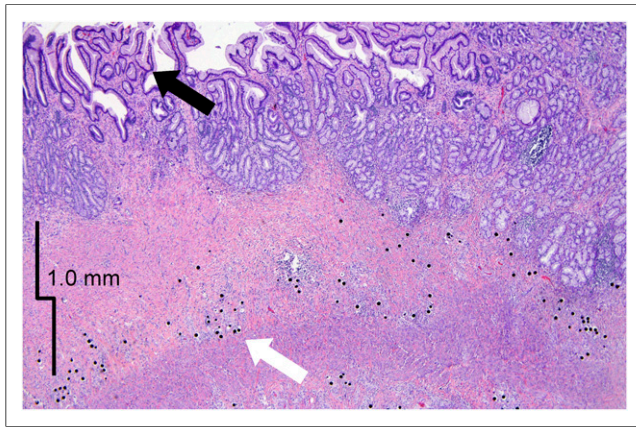


FIGURE 4. H&E section of healed lesion in pig 6. Numerous micro-spheres are visible in submucosa, which is now difficult to identify because of large amount of fibrosis (white arrow). Both normal glandular mucosa and abnormal mucosa with visible changes in glandular activity (black arrow) are present.

Dose Profile Assessment

The thickness of gastric tissue was measured lumen to serosa at every location for which a microsphere cluster was identified. The minimum tissue thickness found was 2.2 mm, with an average thickness of 7.1 mm. A box plot describing the distribution of gastric tissue thickness for each animal is shown in Figure 5. These data were used to determine the accuracy of the MIRSD method for hepatic radioembolization dosimetry applied to the gastrointestinal wall, under the assumption of uniform microsphere deposition within the tissue. At the minimum and average tissue thickness (2.2 and 7.1 mm, respectively), the dose profiles are presented for slab geometry in Figure 6. In both cases under the uniform assumption, D_{avg} overestimates tissue dose at all points in the gastric wall, because CPE will never be achieved at the luminal mucosa and will be achieved only at the center of the gastrointestinal wall if the thickness exceeds the maximum

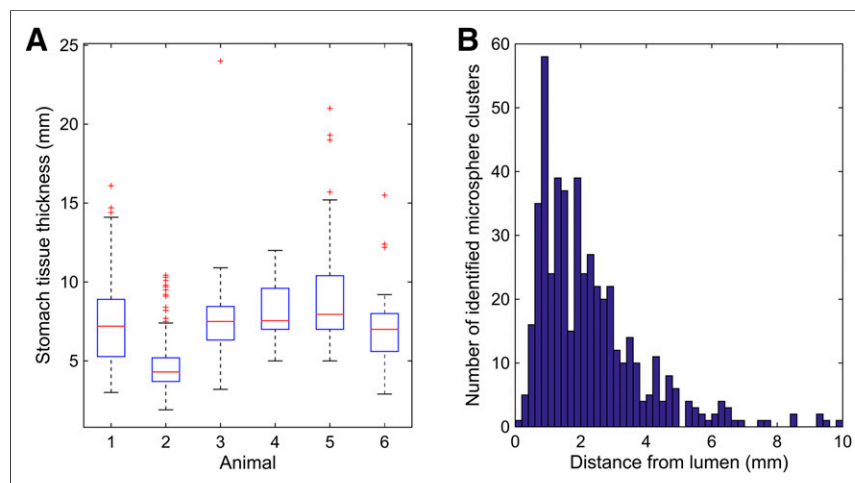


FIGURE 5. (A) Box and whisker plot describing histologic measurement of gastric wall thickness (mucosa to serosa) at points corresponding to microsphere cluster locations in all sections taken from each animal. (B) Histogram detailing distance of each of 467 identified microsphere clusters from luminal mucosa.

range of ^{90}Y β -emissions (11 mm). Under the uniform deposition assumption, the absorbed dose at the luminal mucosa is 37%, 46.5%, and 47% of D_{avg} for a gastrointestinal wall thickness of 2.2, 7.1, and greater than 11.0 mm, respectively.

If the preference for microsphere deposition in the submucosa is accounted for, results change considerably with the absorbed dose at the luminal mucosa, achieving closer agreement with D_{avg} . This dose profile is shown in Figure 7, which, like the spatially dependent deposition of microspheres in Figure 5B, demonstrates an absorbed-dose profile that is highly skewed toward the lumen. Because of the high concentration of microspheres in the submucosa, absorbed dose in this region exceeds D_{avg} by more than 200%, indicated by the dose profile peak in Figure 7. However, once again because of the lack of CPE, absorbed dose falls off quickly nearing the luminal mucosa to 90% of D_{avg} .

The location of the luminal and serosal edges of fibrosis are overlaid on the dose profile in Figure 7. The peak absorbed dose is within the fibrosis band surrounding 94% of measured microsphere clusters. This finding demonstrates physiologic agreement between the absorbed-dose profile (Fig. 7) and resulting biologic effect. Figure 8 shows corresponding H&E and trichrome sections, providing a visual comparison of microsphere location and resulting fibrosis.

DISCUSSION

Using the MIRSD model for hepatic ^{90}Y radioembolization dosimetry, absorbed doses of up to a D_{avg} of 91.9 Gy were delivered to porcine stomach with only superficial injury, which was healing or healed with no medical intervention other than oral Omeprazole. These data may suggest that gastrointestinal tissue toxicity data from EBRT cannot be directly applied to ^{90}Y radioembolization. In addition, the data suggest that clinical cases of severe gastrointestinal ulceration from ^{90}Y radioembolization likely occurred after absorbed doses in excess of 100 Gy. In hepatic radioembolization, in which treatment dosages in excess of 1 GBq are routine, only a small fraction of the treatment dose would need to

be redirected to gastrointestinal tissue to result in a D_{avg} exceeding 100 Gy. This is due to the drastic difference in the volume between the liver and gastrointestinal wall. In particular, for duodenal NTE, for which target volumes may be less than 10 cm^3 , only 20 MBq are necessary to result in a D_{avg} exceeding 100 Gy—just 2% of a modest 1-GBq hepatic treatment dosage.

Although deep ulceration was not appreciated at the doses evaluated, histologic changes including fibrosis in areas of deep mucosa and submucosa matching the tissue depths receiving the highest absorbed dose were seen. This may result in a thinning of the active mucosal layer, which remained intact (Fig. 8) other than in the areas previously described (Table 3). The long-term effects of these fibrotic changes could not be evaluated because of the duration of this study and remain an open potential concern after NTE of ^{90}Y radioembolization to gastrointestinal tissue.

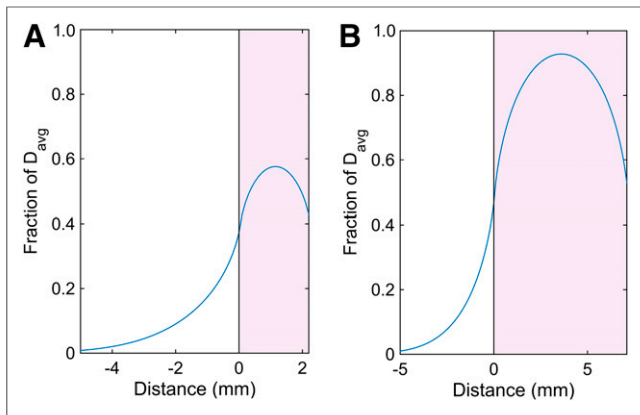


FIGURE 6. Absorbed-dose profiles computed under assumption of uniform deposition within gastric wall and slab geometry. Minimum measured stomach wall thickness (2.2 mm) (A) and average gastric wall thickness (7.1 mm) (B). Shaded area represents gastric wall, and vertical black line indicates luminal mucosa.

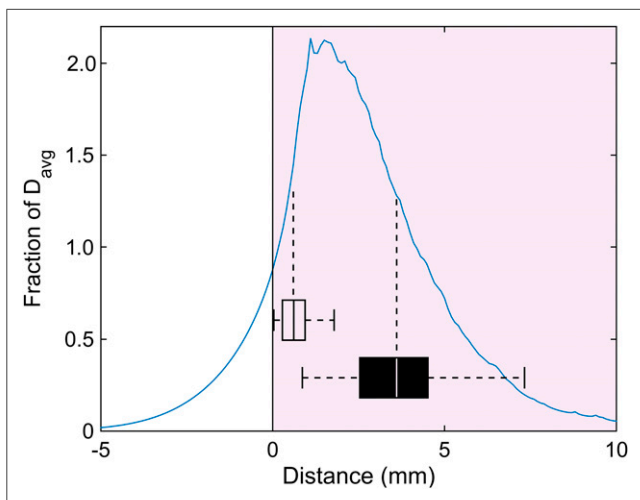


FIGURE 7. Absorbed-dose profile computed using measured spatial microsphere deposition relative to lumen (Fig. 5B). Shaded area represents gastric wall, and vertical black line indicates luminal mucosa. Box and whisker plots denote location of perisubmucosal demarcated edges of fibrotic bands measured on trichrome sections. Fibrotic boundary near lumen (open box) and near serosa (solid box) are plotted and surround tissue areas receiving highest absorbed dose.

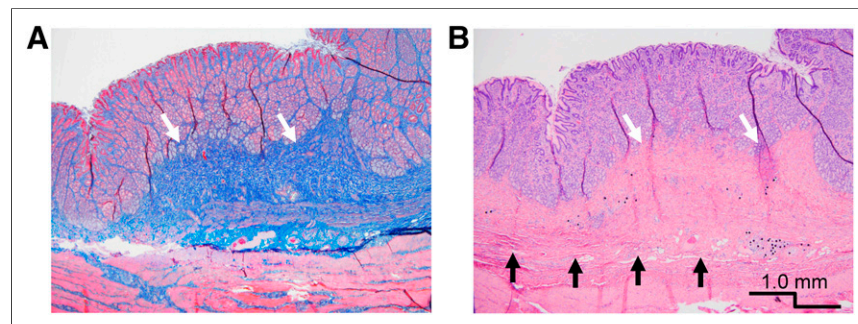


FIGURE 8. Trichrome- (A) and H&E- (B) stained sections of fundus. Predominant submucosal (black arrows) deposition of microspheres is noted with less microspheres in deep mucosa on H&E stain. Fibrosis and thinning of mucosa is visible (white arrows). Remaining glandular mucosa has normal appearance and activity.

When assessing injury to gastrointestinal tissue, the absorbed dose to the luminal mucosa is of highest radiobiologic concern for maintaining acute mucosal integrity. Contrary to hepatic dosimetry, in which tissue volumes are large relative to the range of ^{90}Y β -particles, CPE is not found in the gastrointestinal tract wall because its thickness is generally less than the ^{90}Y β -range. In addition, CPE will never be present at the luminal mucosa after ^{90}Y radioembolization NTE to gastrointestinal tissue. As such, the MIRD hepatic dosimetry method (Eq. 2), which assumes both CPE and uniform microsphere deposition within the compartment of interest, is inherently invalid. As shown in Figure 5, if a uniform deposition within the gastrointestinal wall is assumed, then the lack of CPE at the tissue boundary will result in an overestimation of the absorbed dose at the luminal mucosa by more than a factor of 2 when the MIRD method is used. Unlike hepatic microsphere deposition, however, our data indicate that microsphere deposition within the gastrointestinal wall is not uniform (Fig. 5B). The strong preference for microsphere deposition within the submucosa drastically shifts the dose profile toward the luminal mucosa, resulting in incidental first-order agreement with D_{avg} at the lumen (Fig. 7). Regardless of the deposition pattern of microspheres within the gastrointestinal wall, it is important to emphasize that the lack of CPE at the luminal mucosa boundary results in a sparing effect on these radiosensitive cells, a property inherent to radioembolization, which could partially explain differences between the toxicity data reported here and prior data from EBRT (6). However, this is likely only part of the explanation and as in the liver (11), microdosimetric variation may play a role in the toxicity of ^{90}Y radioembolization in the gastrointestinal tract. To this end, a more detailed microdosimetric investigation is needed.

There are several limitations to this current work. The first and most obvious limitation is that these experiments and observations were performed on pigs. However, pigs have long been used as a surrogate for in vivo experimentation on the effects of ortho-voltage x-rays on skin, with thresholds for injury shown to correspond with clinical observations on humans (17,18). It is likely, but uncertain, that the reported gastrointestinal findings can also be extrapolated to humans with confidence, particularly in light of the histologic similarity between porcine and human gastrointestinal structure.

The second limitation is whether the reported findings can be applied to duodenal NTE, which is more likely to occur clinically. Once again, we can look to toxicity thresholds from EBRT for the duodenum and stomach, which do not appreciably differ (6).

CONCLUSION

The upper gastrointestinal tract may be less sensitive to ^{90}Y radioembolization than previously thought. Lack of CPE at the luminal mucosa contributes to decreased toxicity of ^{90}Y radioembolization compared with EBRT in gastrointestinal tissue. Clinical examples of injury from ^{90}Y NTE have likely resulted from relatively large ^{90}Y activities being deposited in small tissue volumes resulting in absorbed doses in excess of 100 Gy.

DISCLOSURE

The costs of publication of this article were defrayed in part by the payment of page charges. Therefore, and solely to indicate this fact, this article is hereby marked “advertisement” in accordance with 18 USC section 1734. This work was supported by an unrestricted research grant from SIRTEx Medical USA. No other potential conflict of interest relevant to this article was reported.

REFERENCES

1. Lam MG, Banerjee S, Louie JD, et al. Root cause analysis of gastroduodenal ulceration after yttrium-90 radioembolization. *Cardiovasc Intervent Radiol*. 2013;36:1536–1547.
2. Hamoui N, Minocha J, Memon K, et al. Prophylactic embolization of the gastroduodenal and right gastric arteries is not routinely necessary before radioembolization with glass microspheres. *J Vasc Interv Radiol*. 2013;24:1743–1745.
3. Mahvash A, Zaer N, Shaw C, Chasen B, Avritscher R, Murthy R. Temporary balloon occlusion of the common hepatic artery for administration of yttrium-90 resin microspheres in a patient with patent hepatoenteric collaterals. *J Vasc Interv Radiol*. 2012;23:277–280.
4. Fischman AM, Ward TJ, Patel RS, et al. Prospective, randomized study of coil embolization versus surefire infusion system during yttrium-90 radioembolization with resin microspheres. *J Vasc Interv Radiol*. 2014;25:1709–1716.
5. Murthy R, Brown DB, Salem R, et al. Gastrointestinal complications associated with hepatic arterial yttrium-90 microsphere therapy. *J Vasc Interv Radiol*. 2007;18:553–561.
6. Kavanagh BD, Pan CC, Dawson LA, et al. Radiation dose-volume effects in the stomach and small bowel. *Int J Radiat Oncol Biol Phys*. 2010;76:S101–S107.
7. Gunderson LL, Willett CG, Harrison LB, Calvo FA. *Intraoperative Irradiation: Techniques and Results*. New York, NY: Springer; 2011.
8. Kennedy A, Nag S, Salem R, et al. Recommendations for radioembolization of hepatic malignancies using yttrium-90 microsphere brachytherapy: a consensus panel report from the Radioembolization Brachytherapy Oncology Consortium. *Int J Radiat Oncol Biol Phys*. 2007;68:13–23.
9. Lau WY, Kennedy AS, Kim YH, et al. Patient selection and activity planning guide for selective internal radiotherapy with yttrium-90 resin microspheres. *Int J Radiat Oncol Biol Phys*. 2012;82:401–407.
10. Dawson LA, Haken Ten RK, Lawrence TS. Partial irradiation of the liver. *Semin Radiat Oncol*. 2001;11:240–246.
11. Fox RA, Klemp PF, Egan G, Mina LL, Burton MA, Gray BN. Dose distribution following selective internal radiation therapy. *Int J Radiat Oncol Biol Phys*. 1991;21:463–467.
12. Paxton BE, Kim CY, Alley CL, et al. Bariatric embolization for suppression of the hunger hormone ghrelin in a porcine model. *Radiology*. 2013;266:471–479.
13. Gulec SAS, Mesoloras GG, Stabin MM. Dosimetric techniques in ⁹⁰Y-microsphere therapy of liver cancer: the MIRD equations for dose calculations. *J Nucl Med*. 2006;47:1209–1211.
14. Eckerman KF, Westfall RJ, Ryman JC, Cristy M. Availability of nuclear decay data in electronic form, including beta spectra not previously published. *Health Phys*. 1994;67:338–345.
15. Ward DM, Leib MS, Johnston SA, Marini M. The effect of dosing interval on the efficacy of misoprostol in the prevention of aspirin-induced gastric injury. *J Vet Intern Med*. 2003;17:282–290.
16. Campbell AM, Bailey IH, Burton MA. Analysis of the distribution of intra-arterial microspheres in human liver following hepatic yttrium-90 microsphere therapy. *Phys Med Biol*. 2000;45:1023–1033.
17. Archambeau JO, Mathieu GR, Brenneis HJ, Thompson KH, Fairchild RG. The response of the skin of swine to increasing single exposures of 250-KVP X-rays. *Radiat Res*. 1968;36:299–326.
18. Hopewell JW. The skin: its structure and response to ionizing radiation. *Int J Radiat Biol*. 1990;57:751–773.